Finite volume method for radiative heat transfer in an unstructured flow solver for emitting, absorbing and scattering media

2012 J. Phys.: Conf. Ser. 369 012020

(http://iopscience.iop.org/1742-6596/369/1/012020)

Journal of Physics: Conference Series **369** (2012) 012020 doi:10.1088/1742-6596/369/1/012020

Finite volume method for radiative heat transfer in an unstructured flow solver for emitting, absorbing and scattering media

Moncef GAZDALLAH [(1)], Véronique FELDHEIM [(1)], Kilian CLARAMUNT[(2)] and Charles HIRSCH[(2)]

[1] *Faculté Polytechnique de Mons - UMONS, Thermal Engineering and Combustion Laboratory, Rue de l'Epargne 56, 7000 Mons, Belgium.*
[2] *NUMFLO, Rue Descartes, 2 - 7000 Mons – Belgium*

E-mail: moncef.gazdallah@umons.ac.be

Abstract. This paper presents the implementation of the finite volume method to solve the radiative transfer equation in a commercial code. The particularity of this work is that the method applied on unstructured hexahedral meshes does not need a pre-processing step establishing a particular marching order to visit all the control volumes. The solver simply visits the faces of the control volumes as numbered in the hexahedral unstructured mesh. A cell centred mesh and a spatial differencing step scheme to relate facial radiative intensities to nodal intensities is used.
The developed computer code based on FVM has been integrated in the CFD solver FINE^{TM}/Open from NUMECA Int. Radiative heat transfer can be evaluated within systems containing uniform, grey, emitting, absorbing and/or isotropically or linear anisotropically scattering medium bounded by diffuse grey walls. This code has been validated for three test cases. The first one is a three dimensional rectangular enclosure filled with emitting, absorbing and anisotropically scattering media. The second is the differentially heated cubic cavity. The third one is the L-shaped enclosure. For these three test cases a good agreement has been observed when temperature and heat fluxes predictions are compared with references taken, from literature.

1. Introduction

In CFD, finite volume methods are widely used because they ensure conservation laws over the control volume surrounding a node. These methods are also used for convective heat transfer. Finite volume method for radiation (FVM) [1], the numerical technique for solving the radiative transfer equation (RTE), is based on the same control volume technique as used in computational fluid dynamics. Compared with other methods such as zonal method, P_N approximation and Monte Carlo, FVM is thus known to be more compatible with the numerically discretized forms of momentum and energy in nonorthogonal structured or unstructured grids [2, 3]. It transforms the radiative transfer equation to a set of algebraic equations, one for each combination of control volume and solid angle. A differencing scheme that relates a volume facial intensity to a nodal one is required for each

To whom any correspondence should be addressed

direction. A marching order to scan all domain control volumes for each direction is required but it is memory consuming and hard to establish, especially for unstructured meshes.
In this paper, in order to avoid the establishment of this marching order when solving discrete algebraic equations, the solver only visits control volume faces as numbered in the mesh. Each face only limits two control volumes. The use of the "face by face browsing" allows dealing easily with unstructured grids.
Scattering is an important phenomenon in many scientific fields and processes. In combustion chambers, scattering of radiation is mainly due to the presence of particles (e.g. soot). To take scattering into account, anisotropic and linear anisotropic scattering phase functions have been used in the present study.
The computer code developed and integrated in the CFD solver FINE^{TM}/Open from NUMECA Int. calculates the variables needed by the coupling procedure between the radiative transfer and the CFD when solving the energy conservation equation. These variables are the energy radiative source terms and the radiative heat fluxes at the boundaries. The code estimates this information starting from the fields of concentration and temperature provided by the solution of Navier-Stokes equations using a hexahedral mesh. The radiative heat transfer can be evaluated within media containing uniform, grey, emitting, absorbing and/or isotropically or linear anisotropically scattering medium bounded by diffuse grey walls.

2. Finite volume method

2.1. Radiative Transfer Equation (RTE)

The radiation intensity for an absorbing, emitting and scattering grey medium at any position $\vec{r}$ along a path $\vec{s}$ is governed by:

$$\frac{\mathrm{d}I(\vec{r},\vec{s})}{\mathrm{d}s} = -\beta I(\vec{r},\vec{s}) + \kappa I_b(\vec{r}) + \frac{\sigma_s}{4\pi}\int_{\Omega'=4\pi} I(\vec{r},\vec{s}')\Phi(\vec{s}'\rightarrow\vec{s})\,d\Omega' \quad (1)$$

Where κ and σ_s are the absorption and scattering coefficients and $\beta = \kappa + \sigma_s$ is the extinction coefficient. $\Phi(\vec{s}'\rightarrow\vec{s})$ is the scattering phase function for a radiation coming from a direction $\vec{s}'$ to a scattered direction $\vec{s}$. For grey diffusely reflecting walls, the radiative intensity emitted into the medium from the boundary at a point r is given by:

$$I(\vec{r}_w) = \varepsilon(\vec{r}_w)I_b(T(\vec{r}_w)) + \frac{1-\varepsilon(\vec{r}_w)}{\pi}\int_{\vec{s}'.\vec{n}_w<0} I(\vec{r}_w,\vec{s}')\left|\vec{s}'.\vec{n}_w\right|d\Omega' \quad (2)$$

Where $\vec{n}_w$ is the local unit outward normal vector, $\varepsilon(\vec{r}_w)$ is the wall local emissivity and $I_b(\vec{r}_w)$ the blackbody radiation intensity at the local temperature of the wall.

2.2. Principle

In the FVM formulation [1, 2, 3], the domain is divided into a number of control volumes; for each one, the radiative intensity is located at the centre. The solid angle, 4π steradians, is discretized into N=N_θ.N_φ directions. θ is the polar angle ranging from 0 to π and φ is the azimuthal angle ranging from 0 to 2π. A set of discretized linear equations is obtained by integrating the radiative heat transfer equation over the whole domain. The resolution of the radiative transfer equation for each direction M (M=1…N) allows to obtain the directional intensities I_M. Associated with control solid angles, they are used to evaluate the radiative source terms and wall heat fluxes.

2.2.1. Angular discretization

A discrete direction $\vec{s}_i$ is defined by the polar angle θ_m and the azimuthal angle φ_n and has the following form:

$$\vec{s}_i = \sin\theta_m \sin\varphi_n \vec{i} + \sin\theta_m \cos\varphi_n \vec{j} + \cos\theta_m \vec{k} \quad (3)$$

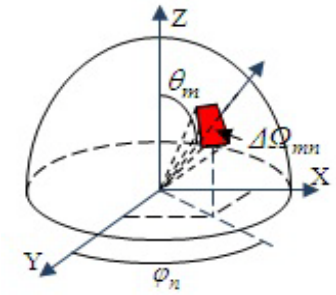

Figure 1: Control solid angle.

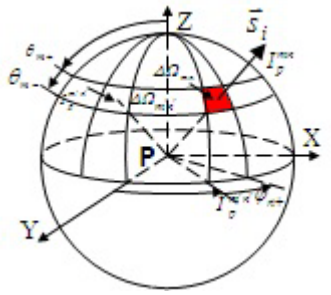

Figure 2: Control solid angle limits.

The subscripts *m* and *n* represent, respectively, the number of polar angles and azimuthal angles associated with the direction $\vec{s}_i$. Although the control solid angle can be defined arbitrarily [5] in the present study a uniform angular discretization is used:

$$\Delta\theta_m = \theta_{m+} - \theta_{m-} = \pi / N_\theta \quad , \quad \Delta\varphi_n = \varphi_{n+} - \varphi_{n-} = 2\pi / N_\varphi \quad , \quad \theta_m = \theta_{m+} - \Delta\theta_m / 2 \quad , \varphi_n = \varphi_{n+} - \Delta\varphi_n / 2 \tag{4}$$

2.2.2. Finite volume formulation

Integration of equation (1) over a given control volume V_p and control solid angle $\Delta\Omega_{mn}$ is done by assuming that the magnitude of the intensity is constant but its direction varies within the control volume V_p and control solid angle $\Delta\Omega_{mn}$. The following finite volume formulation can be obtained (N_f is the number of faces limiting the control volume and A_j the surface areas) [28]:

$$\sum_{j=1}^{Nf} I_j^{mn} A_j D_{i,j}^{mn} = \beta\left[-I_p^{mn} + S_R^{mn}\right] V_p \, \Delta\Omega_{mn} \tag{5}$$

$$S_R^{mn} = (1-\omega) I_{b,p} + \frac{\omega}{4\pi} \sum_{m'=1}^{N} I_p^{m'n'} \overline{\Phi}_{m'm} d\Omega_{m'} \tag{6}$$

$$D_{i,j}^{mn} = \int_{n\Delta\Phi}^{(n+1)\Delta\Phi} \int_{m\Delta\theta}^{(m+1)\Delta\theta} (\vec{s}_i . \vec{n}_j) \sin\theta \, d\theta \, d\phi \tag{7}$$

$\omega = \frac{\sigma_s}{\beta}$ is the scattering albedo and $D_{i,j}^{mn}$ is the directional weight.

For a given control volume and a given direction $\vec{s}_i$, equation (5) represents an algebraic equation where the unknowns are the values of the intensity I_p^{mn} related to the control volume and the values of the intensities I_j^{mn} at its faces. In order to solve this equation, a spatial differencing scheme must be selected to link control volume faces intensities I_j^{mn} to a nodal one.

2.2.3. Differencing scheme

A weighted difference scheme is very useful in the case of unstructured meshes [6, 7, 8, 9, 10 and 11]. It is based on the following formulation:

$$I_p^{mn} = \alpha I_{j,out}^{mn} + (1-\alpha) I_{j,in}^{mn} \tag{8}$$

Where α is a weighting factor ranging from 0 to 1. Following a direction $\vec{s}_i$, $I_{j,in}^{mn}$ and $I_{j,out}^{mn}$ are a couple of faces intensities, respectively entering ($D_{i,j}^{mn} < 0$) and leaving ($D_{i,j}^{mn} > 0$) the control volume V_p. For any face j of a control volume V_p, the following expression can be written:

$$D_{i,j}^{mn} I_j^{mn} = \max(D_{i,j}^{mn}, 0) I_{j,out}^{mn} - \max(-D_{i,j}^{mn}, 0) I_{j,in}^{mn} = D_{i,j,out}^{mn} I_{j,out}^{mn} + D_{i,j,in}^{mn} I_{j,in}^{mn} \tag{9}$$

From equation (8), $I_{j,out}^{mn}$ can be written as:

$$I_{j,out}^{mn} = \frac{I_p^{mn}}{\alpha} + \frac{(\alpha - 1)}{\alpha} I_{j,in}^{mn} \tag{10}$$

By considering equations (5, 8, 9 and 10) and after some arrangements, the following general linear system of equations can be obtained:

$$a_p^{mn} I_p^{mn} = \sum_{j=1}^{N_f} a_j^{mn} I_{j,in}^{mn} + b_p^{mn} \tag{11}$$

Where

$$a_p^{mn} = \sum_{j=1}^{Nf} A_j \frac{D_{i,j,out}^{mn}}{\alpha} + \beta V_p \Delta\Omega_{mn}, \quad a_j^{mn} = -A_j \left(D_{i,j,out}^{mn} \frac{(\alpha - 1)}{\alpha} + D_{i,j,in}^{mn} \right), b_p^{mn} = \beta S_R^{mn} V_p \Delta\Omega_{mn} \tag{12}$$

Equation (11) is an algebraic equation relating intensity I_p^{mn} at the control volume centre to the entering intensity $I_{j,in}^{mn}$. The boundary condition in equation (2) for a diffusely emitting and reflecting wall can be derived easily as:

$$I_w^{mn} = \varepsilon_w I_{bw} + \frac{1 - \varepsilon_w}{\pi} \sum_{\vec{s}_i' . \vec{n}_w < 0} I_w^{m'n'} \left| D_{i,w,in}^{m'n'} \right| \tag{13}$$

Where

$$D_{i,w,in}^{mn} = \int_{\Delta\Omega_{mn}} (\vec{s}_i . \vec{n}_w) \, d\Omega \qquad \vec{s}_i . \vec{n}_w < 0 \tag{14}$$

$D_{i,w,j}^{mn}$ and I_w^{mn} are, respectively, the directional weight and the intensity at the boundary wall. Equation (11) for each node, together with boundary conditions, provides the equations set for the nodal intensities in direction $\vec{s}_i$. Similar set of equations are formed for the other directions.

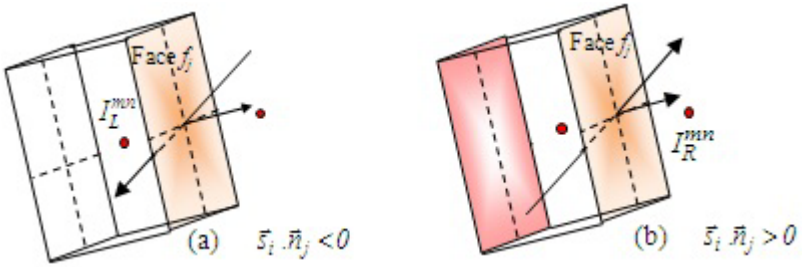

Figure 3: Inflow and outflow radiation through a control volume face.

Considering the face f_j in figure 3, where I_L^{mn} is the nodal intensity at the centre of the control volume located at the left and I_R^{mn} is the nodal intensity at the centre of the control volume located at the right, following the sign of the scalar product $\vec{s}_i . \vec{n}_j$, the following can be stated:

If $\vec{s}_i . \vec{n}_j < 0$: radiation transmitted from the right control volume to the left control volume through the face f_j is: $I_{j,out}^{mn} = \frac{I_R^{mn}}{\alpha} + \frac{(\alpha - 1)}{\alpha} I_{j,in}^{mn}$ if α=1 $I_{j,out}^{mn} = I_R^{mn}$

If $\vec{s}_i . \vec{n}_j > 0$: radiation transmitted from the left control volume to the right control volume through the face f_j is $I_{j,out}^{mn} = \frac{I_L^{mn}}{\alpha} + \frac{(\alpha - 1)}{\alpha} I_{j,in}^{mn}$ if α=1 $I_{j,out}^{mn} = I_L^{mn}$

α = 1 corresponds to the step scheme which states that, for a given control volume Vp and direction $\vec{s}_i$, the value of the intensity at any face of the control volume is assumed equal to the value of the intensity at the centre of the nearest control volume placed upstream of the direction $\vec{s}_i$. Then, it can be equal to the value in the neighbouring control volume or to the value of the control volume Vp. By using this differencing scheme, the calculation can be done face by face.

2.2.4. Control volume faces browsing

In a control volume faces browsing method, the solver visits the faces of the control volumes as numbered in the mesh. To record the exchange between control volumes across each visited face, the equation (11), relating intensity I_p^{mn} at the control volume centre to the entering radiant intensity at its faces, is transformed as a ratio between two terms ($T_{1,p}^{mn}$, $T_{2,p}^{mn}$). From equations (11) and (12) the following expression can be written:

$$I_p^{mn} = \frac{T_{1,p}^{mn}}{T_{2,p}^{mn}} \tag{15}$$

Where

$$T_{1,p}^{mn} = T_{1,p,0}^{mn} + \sum_{j=1}^{N_f} a_j^{mn} I_{j,in}^{mn} \quad with \quad T_{1,p,0}^{mn} = S_R^{mn} \beta V_p \, \Delta\Omega_{mn} \tag{16}$$

and

$$T_{2,p}^{mn} = T_{2,p,0}^{mn} + \sum_{j=1}^{Nf} A_j D_{i,j,out}^{mn} \qquad with \; T_{2,p,0}^{mn} = \beta V_p \, \Delta\Omega_{mn} \tag{17}$$

Each term $T_{1,p}^{mn}$ or $T_{2,p}^{mn}$ consists of two parts. The first one depends on the geometric and radiative properties of the control volume and angular discretization. The second one is the sum of the entering intensities across the faces of the control volume. The source term S_R^{mn} is included into the first part of $T_{1,p}^{mn}$. An iterative procedure is needed to compute the whole field of the intensities I_p^{mn} in the case of diffusely reflecting walls. Once the intensity field is obtained, the wall radiative heat flux can be obtained as follows:

$$q_w = \sum_{m=1}^{N_\theta} \sum_{n=1}^{N\varphi} I_w^{mn} (D_{i,w,in}^{mn} + D_{i,w,out}^{mn}) = \sum_{m=1}^{N_\theta} \sum_{n=1}^{N\varphi} I_w^{mn} (-\max(-D_{i,w}^{mn},0) + \max(D_{i,w}^{mn},0)) \tag{18}$$

For a given control volume, the incident radiation G_p evaluated at its centre P is calculated as follows:

$$G_p = \int_{4\pi} I(\vec{r},\vec{s}) d\Omega = \sum_{m=1}^{N_\theta} \sum_{n=1}^{N\varphi} I_p^{mn} \Delta\Omega_{mn} \tag{19}$$

The source term S_r is calculated as follows:

$$S_r = k_a \left[4\pi . I_{p,b} - G_P \right] \tag{20}$$

2.2.5. Scattering phase functions

For isotropic scattering the phase function $\mathbf{\Phi}(\vec{s}', \vec{s})$ is equal to 1 while for linear isotropic scattering, the following expression can be written:

$$\begin{aligned} &\Phi(\mu_p) = 1 + a\mu_p \quad with \quad -1 < a <= 1 \\ &\mu_p = cos(\Psi) \end{aligned} \tag{21}$$

Ψ is the angle between incoming direction $\vec{s}$ and scattered direction $\vec{s}'$ [12].

3. Test cases: results and discussion

The code is tested for enclosures of simple geometry already studied by other authors. The first test refers to a three dimensional rectangular enclosure also called ideal furnace studied by Truelove [14,15] for emitting, absorbing and/or anisotropically or isotropically scattering media. The second is a differentially heated cavity, studied by many investigators using different methods [16, 17 and 18]. The third one is a L-shaped enclosure studied by Malalasekera et al using the discrete transfer method [19].

3.1. Three dimensional enclosure

The three-dimensional rectangular enclosure (see figure 5) is considered filled with grey absorbing emitting and/or scattering medium. Its dimensions are 2m x 2m x 4m – in the x, y and z direction respectively. As shown in figure 5, small walls are at 1200 and 400 K while the other four walls are

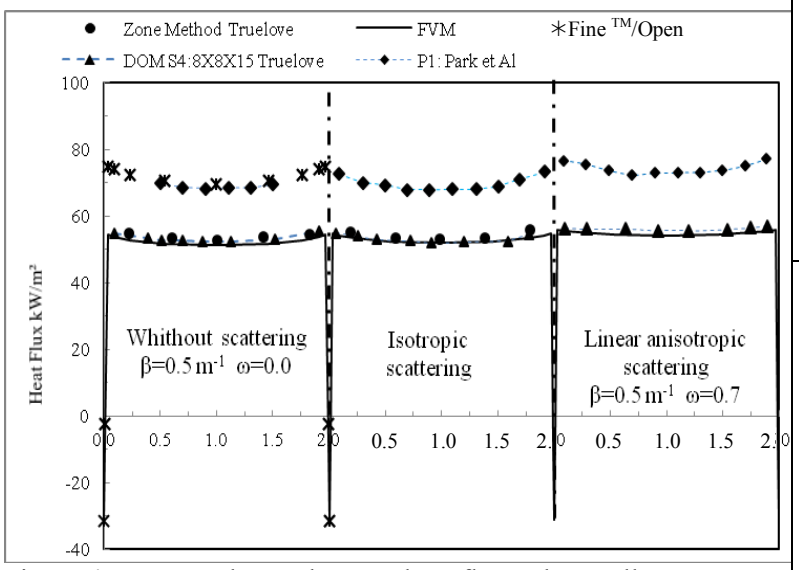

Figure 4: Rectangular enclosure - heat flux at hot wall.

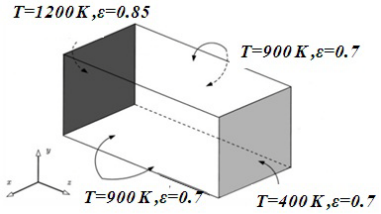

Figure 5: Boundary conditions.

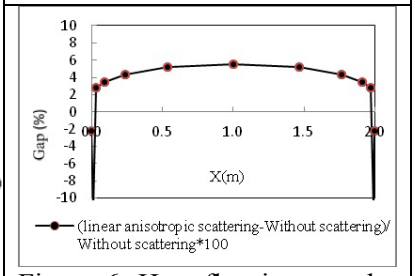

Figure 6: Heat flux increase by linear anisotropic scattering at hot wall (y=1, z=0).

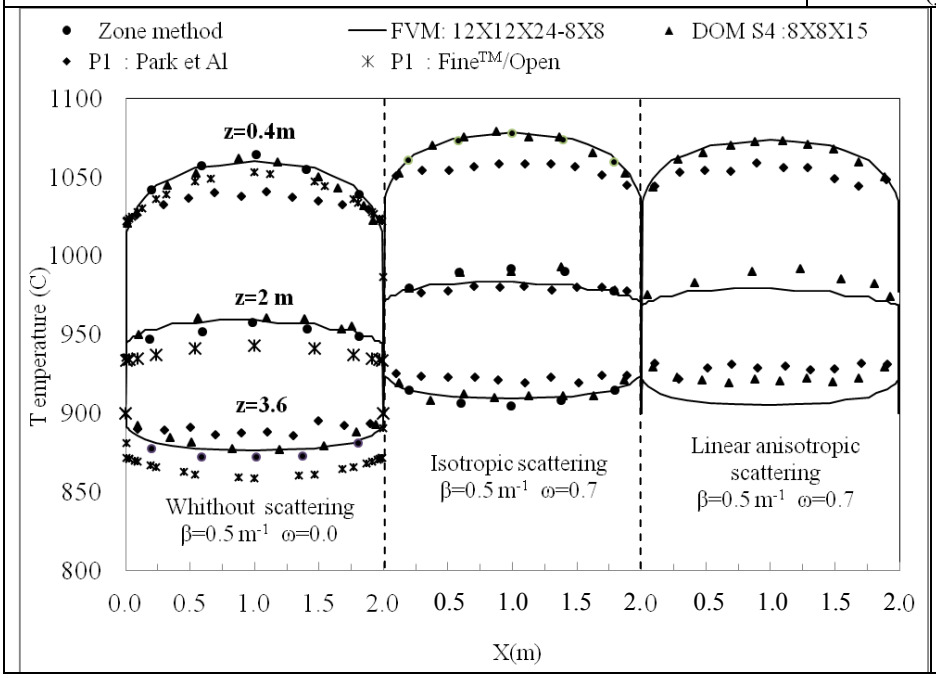

Figure 7: Comparison of temperature profiles, at y=1 and three z locations, from FVM, Zone method [14], DOM S4 [14] and P1 Park [24], P1 FINE™/Open from NUMECA Int, for three phase functions: without scattering, isotropic and linear anisotropic scattering.

maintained at 900 K. The walls are supposed to reflect and emit diffusively, and to have emissivities of 0.85 for the hottest wall and 0.7 for the remaining walls [22]. In this problem, conduction and convection effects are neglected. Hence, the medium is assumed to be at radiative equilibrium with an additional homogeneous heat source $S = 5kW/m^3$. The radiative equilibrium condition implies that the only term in the energy equation is the divergence of the radiative heat flux. In the presence of a source term S, the energy equation is simply written as:

$$\vec{\nabla} \cdot \vec{Q}_r + S = 0 \tag{25}$$

Two phase functions are tested: isotropically and linear anisotropically scattering medium corresponding to an extinction coefficient $\beta = k_a + \sigma_s = 0.5$ and a scattering albedo $\omega = 0.7$.

Results calculated by Finite Volume Method (FVM) are performed with a (12x12x24) mesh and 64 directions (N_θ=8 and N_φ=8). For isotropic scattering, comparison in figure 4 shows a good agreement of the FVM results with those of zone method and DOM S4 [14]. For linear anisotropic scattering the agreement of the FVM and DOM S4 is also good. However, results of P1 method [24] denote a significant difference with the zonal and DOM S4 methods.

As explained by Truelove [14], the effect of isotropic scattering is an increase of the emissive power σT^4 by $\omega \nabla .q /(4\beta(1-\omega))$, while the heat flux distribution is unchanged for specified radiative flux in the medium. The FVM results given in figure 4 are consistent with this explanation.

Linear anisotropic scattering increases the absolute value of the heat flux by about 5% at the walls as shown in figure 6. This effect is to be expected because the net radiative flux is directed from the hot to the cold surface (in the + z direction) and is enhanced by forward scattering (a=1). Comparison in figure 7 shows a good agreement of the temperature profiles calculated by FVM, the zone method [14], and DOM S4 [14], for the case of purely emitting and absorbing media and isotropically scattering media. However, for linear anisotropic scattering, the gap between FVM and DOM S4 is more pronounced near the cold wall. P1 results by Park [24] and by FINE^{TM}/Open from NUMECA Int. denote a significant difference with the zonal, FVM and DOM S4 methods for the three cases. Compared to the case without scattering, isotropic scattering increases temperature profiles by increasing uniformly throughout the medium the emissive power σT^4 by $\omega \nabla .q /(4\beta(1-\omega))$, while linear anisotropic scattering tends to make temperature distribution more uniform than isotropic scattering.

3.2. Differentially heated cavity

For this case, the study is focused on combined radiation and natural convection for different optical thicknesses and different Rayleigh numbers for the case of purely absorbing, emitting grey medium in a cubic enclosure with sides of unit length L=1m. Scattering is neglected according to the previous results in the literature [18, 25 and 26] which state that scattering has hardly any effect on the heat transfer in this case. As shown in figure 9, the two opposite side walls of the enclosure are kept at a different temperature. The "west" wall is at T_h, the "east" wall at T_c with $T_h > T_c$ while the others are adiabatic. All walls are treated as black bodies (ε=1). To characterize the medium, the following assumptions are considered:

- The flow is laminar, newtonian, and incompressible
- The thermophysical properties of the fluid are constant and a Boussinesq variable density formulation is used to incorporate change in density due to temperature difference. The density is also constant in all the terms of the Navier-Stokes equations except for the buoyancy term.

The strategy of the Navier Stokes equations (NSE) and radiative transfer equation (RTE) solution is stated as follows:

1. Initialize the velocity, temperature, and intensity field
2. Solve the RTE from the current temperature field for a fixed number of iteration

3. Compute the radiative source term
4. Solve the coupled velocity and temperature field with the above radiative source term
5. Update the temperature field
6. Repeat 2 to 5 until the convergence of the solution of the Navier-Stokes equations and the RTE.

Dimensionless convective (Q_C^*) and radiative (Q_R^*) heat fluxes called also, respectively, convective and radiative Nusselt number are calculated as follows:

$$Q_C^* = -\frac{L}{\Delta T}\frac{\partial T^*}{\partial x^*} \qquad Q_R^* = \frac{LQ_R}{k\Delta T} \tag{26}$$

Where L is the side length, $T_0^* = T_c / \Delta T$ the reference temperature ratio (fixed to 17) and $\Delta T = T_h - T_c$.

For this study, the Planck number $Pl = k\Delta T/(L\sigma T_c^4)$, where k is the convection coefficient and σ the Stephan-Boltzman constant, is fixed to Pl=0.016. The Prandtl number is fixed to Pr= 0.71. Tables 1 and 2 show average of dimensionless convective and radiative heat fluxes at the hot wall for three Rayleigh numbers and 3 different optical thicknesses (τ) in a range from 1 to 30 evaluated by four methods. The agreement of the FT_n-FVM [27], DOM S4 [16] and FVM is good for radiation and convection. As expected, for low optical thicknesses, the P1 method denotes a significant difference with FT_n-FVM [27], DOM S4 [16] and FVM for the evaluation of average of dimensionless radiative heat fluxes.

In FT_n FVM the polar angle is divided uniformly into an even number, n, while the azimuthal angle is uniformly divided so that the total number of the control angles, N, is given as n(n + 2), which is the same as the number of the discrete ordinate directions of the S_N DOM. More details on FT_n-FVM can be found in [27].

Table 1. Dimensionless average convective heat flux at hot wall Q_C*: meshing 33x33x33, N_θ =4, N_φ=4

	τ=1				τ=10				τ=30			
Rayleigh	FT_n - FVM	DOM	FVM	P1	FT_n - FVM	DOM	FVM	P1	FT_n - FVM	DOM	FVM	P1
$Ra=10^4$	2.45	2.25	2.46	3.48	2.23	2.11	2.30	2.24	*	2.08	2.23	2.11
$Ra=10^5$	4.04	3.92	4.10	4.69	4.46	4.21	4.27	4.40	*	4.34	4.45	4.39
$Ra=10^6$	*	7.63	7.67	7.83	*	8.28	8.08	8.34	*	8.68	8.50	8.69

Table 2. Dimensionless average radiative heat flux at hot wall Q_R*: meshing 33x33x33, N_θ=4, N_φ=4

	τ=1				τ=10				τ=30			
Rayleigh	FT_n - FVM	DOM	FVM	P1	FT_n - FVM	DOM	FVM	P1	FT_n - FVM	DOM	FVM	P1
$Ra=10^4$	5.12	4.69	5.35	8.40	1.65	1.54	1.87	1.63	*	0.79	0.86	0.66
$Ra=10^5$	5.88	5.44	5.98	8.81	2.99	2.80	3.06	2.97	*	1.60	1.65	1.35
$Ra=10^6$	*	6.25	6.74	9.43	*	4.36	4.52	4.69	*	2.86	2.80	2.48

Profiles of dimensionless average total heat flux versus dimensionless depth Z/L at the hot wall in figure 8 confirm the agreement of results of both methods; DOM S4 from Colomer [16] and FVM. They also show that the radiative heat flux at the hot wall decreases as the optical thickness increases. Isothermal surfaces in figure 9, calculated for four Rayleigh numbers and an optical thickness τ=1, show that for low Rayleigh numbers the conduction heat transfer prevails and the isotherms are nearly vertical (parallel to the gravity field). For high Rayleigh numbers, the isotherms become more horizontal, since the natural convection term, which dominates the conductive term, tends to convey the hottest fluid above the coldest. Thus the isotherms are nearly horizontal (perpendicular to gravity field) in the middle region of the enclosure [16].

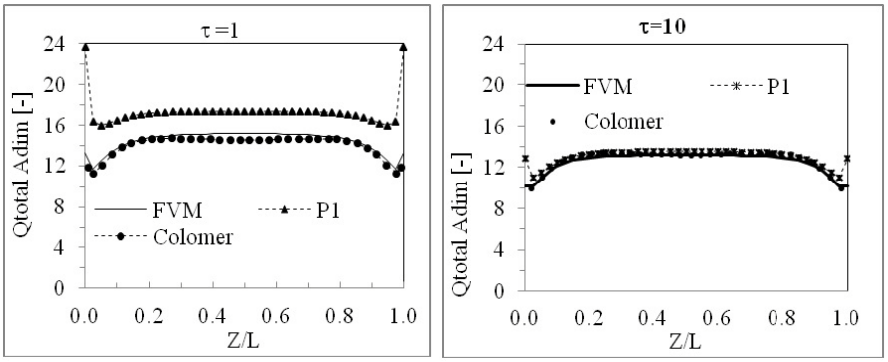

Figure 8: Average total heat flux along Y axes versus dimensionless depth Z/L at the hot wall Meshing:33x33x33, N_θ=4, N_φ=4 Rayleigh =10^6

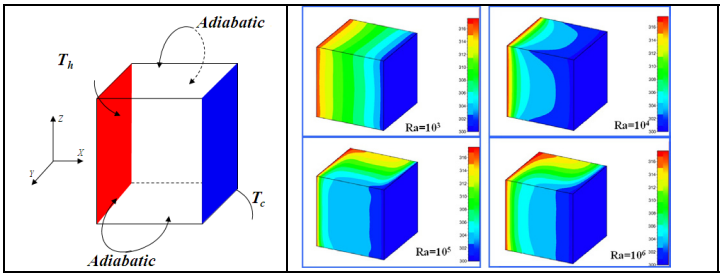

Figure 9: Isothermals surfaces distribution for τ=1.

3.3. L-shaped enclosure

In order to test the code in the case of enclosures with arbitrary geometry a L-shaped enclosure [19, 20, 22 and 23] containing an emitting-absorbing medium at a temperature of 1000 K is considered (see figure (10)). The walls are black at 500 K. Figure (11) shows the evolution of the predicted net heat flux along the A-B line (marked on figure 10) for five values of the absorption coefficient of the medium. Results calculated by FVM are performed with a mesh of 16384 control volumes and 16 directions (N_θ =4 and N_φ=4).The FVM predictions are in good agreement with those of Malalasekera et al [20] who used the discrete transfer method with a body-fitted grid arrangement to discretize the enclosure and 16x16 rays for angular discretization.

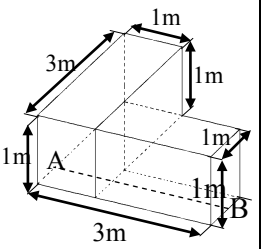

Figure 10: L-shaped enclosure.

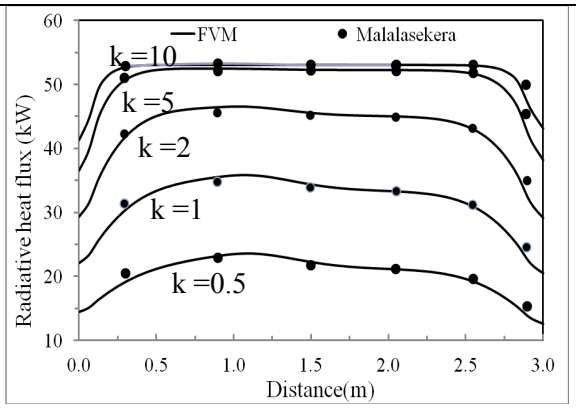

Figure 11: Radiative heat fluxes along the line A-B, shown in figure 10, for five values of absorption coefficients k.

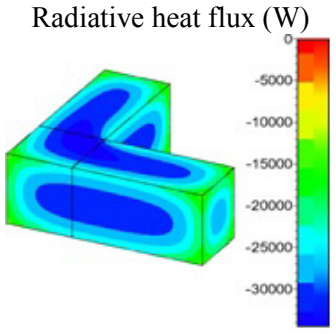

Figure 12: Radiative heat flux distribution at walls. (absorption coefficient k=1)

4. Conclusion

In this study, a finite volume method (FVM) is developed and used to predict three-dimensional radiative heat transfer within an absorbing, emitting and scattering media without a need to a pre-processing step establishing a particular marching order to visit all the control volumes. The developed computer code based on this method is integrated in the unstructured CFD solver FINE™/Open from

NUMECA Int. Then it is applied to three types of enclosures. In the first enclosure, the effects of isotropic and linear anisotropic scattering is investigated and results show that linear anisotropic scattering increases the absolute value of the heat flux. In the second enclosure, the study of combined radiation and natural convection for different optical thicknesses and different Rayleigh numbers shows that heat transfer is dominated by the radiation for lower optical thicknesses. When Rayleigh number increases, the natural convection term dominates the conductive term and isotherms become more horizontal. In the third enclosure, the effect of the shape of the enclosure is studied. For the three enclosures, calculated results are compared with the zone method, discrete ordinates method (DOM) or discrete transfer method from the literature. A good agreement has been observed for both temperature and heat fluxes predictions by the FVM. As expected, the comparison between FVM and P1 shows that the FVM is more accurate for lower optical thicknesses and as accurate as P1 for higher values. Thus, integration of the FVM in FINE^{TM}/Open from NUMECA Int. leads to accurate prediction of the variables needed by the coupling procedure between the radiative transfer and the CFD when solving the energy conservation equation.

Acknowledgments
The authors would like to acknowledge the financial support of the Ministère de la Région Wallonne, in the framework of research program Multi-Φ of the Plan Marshall. The authors express their acknowledgement to NUMECA Int. for their collaboration in carrying out this work.

References
[1] Raithby GD and Chui EH, 1990 *J. Heat Transfer*, **112** 415–423
[2] Raithby GD and Chui EH, 1993 *Num. Heat Transfer*, B 23 269–288
[3] Raithby GD, 1999 *Numer Heat Transfer*, B 35 389–405
[4] Jendoubi S and Lee HS, 1993 *J. Thermophys and. Heat transfer* 7 213-219
[5] Murthy JY and Mathur SR. 1998 *J. Thermophys and. Heat transfer* 12 313–321
[6] Borges De Miranda A and Sacadura JF, 1996 *J. Heat Transfer* **118** 650–653
[7] Cheong KB and Song TH, 1995 *Num. Heat Transfer* **B 27** 155–173
[8] Jamaluddin AS and Smith P J, 1988 *Combust. Sci. Technol*. **59** 321
[9] Lathrop KD, 1969 J. Comput. Phys. 4 475
[10] Joseph D, El Hafi M, Fournier R and Cuenot B , 2005 *Int. J. of Thermal Sciences* **44** 851–864
[11] Capdevila R , Pérez-Segarra CD and Oliva A, 2010, JQSRT, **111 (2)** 264–273
[12] Chiao MC and Churchill S W , 1955 *J. Opt. Soc. Am.* **45**, 958-961
[13] Chai JC and Patankar SV, 2000 *Advances in Numer. Heat Transfer* **vol 4** ed Taylor and Francis
[14] Truelove JS, 1988*, J. Quant. Spec. and Rad. Heat Transfer* **39** 27-31
[15] Grissa H, Askri F, Ben Salah M and Ben Nasrallah S, 2007 *JQSRT* **105(3)** 388–404
[16] Colomer G, Costa M, Consul R and Oliva A, 2004 *Int. J. of Heat and Mass Transfer* **47** 257-269
[17] Borjini MN, Aissia HB, Halouani K, and Zeghmati B, *2008 Int. J. Heat Fluid Flow*, **29** 107-118
[18] Kumar P and Eswaran V, 2010 *J. Heat Transfer*, **132** 023501-1-023501-13
[19] Malalasekera WMG and James EH*,* 1996 *J. Heat transfer* **118** 225-227
[20] Grissa H, Askri F, Ben Salah M and Ben Nasrallah S, 2010 *JQSRT* **111(1)** 144–154
[21] Wang CA,Sadat H, Ledez V and Lemonnier D, 2010 *IJTS* **49(12)** 2282–2288
[22] Mengüç M and Viskanta R, 1985, *J. Quant. Spec. and Rad. Heat Transfer* **33** 533-549
[23] Grissa H, Askri F, Ben Salah M and Ben Nasrallah S, 2011 *JQSRT* **112** 2661-2675
[24] Park HM and Ahluwalia RK and Im KH, 1993 *Int. J. of Heat and Mass Transfer* ***36-5,*** 1181-1189
[25] Tan Z and Howell JR, 1991 *Int. J. of Heat and Mass Transfer* **34 (3)** 785-793
[26] Mondal B and Mishra SC, 2009 *Num. Heat Transfer*, **Part A 55** 18–41
[27] Kim SH and Huh KY, 2000, *Int. J. of Heat and Mass Transfer **43,*** 1233-1242
[28] Kim MY, Baek SW and Park JH, 2001 *Num. Heat Transfer*, **Part B 39** 617–635